SPH Simulations of Dam-break Flows around Movable Structures

Wei Jian and Dongfang Liang*
Department of Engineering, University of Cambridge
Cambridge, UK

Songdong Shao#
Department of Civil and Structural Engineering, University of Sheffield
Sheffield, UK

Ridong Chen and Kejun Yang
State Key Laboratory of Hydraulics and Mountain River Engineering, Sichuan University
Chengdu, China

In this paper, 3D weakly compressible and incompressible Smoothed Particle Hydrodynamics (WCSPH & ISPH) models are used to study dam-break flows impacting on either a fixed or a movable structure. First, the two models' performances are compared in terms of CPU time efficiency and numerical accuracy, as well as the water surface shapes and pressure fields. Then, they are applied to investigate dam-break flow interactions with structures placed in the path of the flood. The study found that the ISPH modelling approach is slightly superior to the WCSPH approach, since more stable particle motion and pressure distribution can be achieved with reasonable CPU load.

KEY WORDS: 3D, ISPH, WCSPH, dam-break flow, fluid-structure interaction, movable structure.

INTRODUCTION

Monaghan (1994) first extended the SPH modelling concept to incompressible flows with free surface using a weakly compressible assumption. An equation of state was used to link the density with the pressure field, which is the commonly-used WCSPH approach. Since then, it has been found that the SPH method has a great potential for problems involving large deformation of free surfaces, moving interfaces and deformable boundaries. For example, Gómez-Gesteira and Dalrymple (2004) reproduced the impact of a dam-break flow on a tall structure using a 3D WCSPH model. In addition, even though the SPH modelling technique has been widely used in the research community, very few engineering applications have been reported due to its relatively high computational cost. Recent work in the parallelisation of the SPH code could enable some realistic simulations to be possible (Ferrari *et al*., 2009).

Despite being very effective in the water-surface tracking, the conventional WCSPH method has been found to suffer from the unphysical fluctuations in the pressure prediction. This is caused by the small density errors in the calculation, which could be amplified through the equation of state. Some effective treatments have been made to correct the density and kernel gradient errors, which proved to significantly improve the WCSPH simulation capacity. On the other hand, quite a few incompressible models with better stability properties have been established. For example, Cummins and Rudman (1999) were the pioneers to put forward the projection SPH (PSPH) method, who imposed a zero-divergence requirement in the derivation of the pressure Poisson equation. Follow-on development on the PSPH method leads to the divergence-free ISPH models. Besides, following the principles of the Moving Particle Semi-implicit (MPS) method (Koshizuka *et al*., 1998; Gotoh and Sakai, 1999), in which the constant-density condition was used to derive the PPE to enforce the incompressibility requirement, Shao and Lo (2003) proposed the density-invariant ISPH method. Further improvement was made by Hu and Adams (2009) who combined the velocity divergence-free and density-invariant algorithms together.

Comparisons on the performance of various WCSPH and ISPH approaches have always been a debate over the years. Cummins and Rudman (1999) simulated a vortex spin-down and Rayleigh-Taylor instability and they found that the PSPH method produced more accurate results with better computational efficiency for the low and medium particle resolutions. More detailed comparisons and evaluations of different SPH modelling techniques as well as their potential improvements were reported by Khayyer and Gotoh (2010) for the dam-break flow over a wet bed.

This paper's purpose is two-fold. First, we would like to make an objective comparison between the two standard SPH modelling approaches, i.e. WCSPH and ISPH. Although Chen *et al*. (2013) found that the improved WCSPH is more attractive than the standard SPH approach, we need to take caution that the two methods should have been compared on an equal footing. For example, some relevant numerical treatments, such as the density normalizations and kernel/kernel gradient corrections, should be disabled in the WCSPH. Another objective is to use an improved ISPH pressure algorithm to investigate the 3D dam-break flow interactions with fixed and movable structures. Although quite a few 2D ISPH applications have been reported concerning similar problems, very little work has been undertaken using the 3D approach. One reason could be the long CPU time, as the computational cost increases rapidly with the size of the PPE matrix and an extra dimension drastically increases the number of coupled equations. Another reason could be attributed to the stability of the ISPH predictions of the pressure and particle position. As reported in Gotoh *et al*. (2005), the standard 2D solid boundary treatment in the MPS method could lead to fluid particle penetrations into the solid wall. Therefore, our study also aims to explore the potentials of the ISPH simulation in complex 3D flows.

Since the pioneering study of the wedge entry into water with the WCSPH method (Oger *et al.*, 2006) and the float motion with the Moving Particle Semi-implicit method (Koshizuka *et al.*, 1998), more and more researches have been carried out to investigate the interaction between the solid objects and flows. Some studies even consider multi-degrees of the freedom, as documented by Bouscasse *et al.* (2013), Liu *et al.* (2014), Amicarelli *et al.* (2015), Ren *et al.* (2015) and Canelas *et al.* (2015).

*ISOPE member #Correspondence author

GOVERNING EQUATIONS AND SPH PRINCIPLES

All kinds of the SPH models solve the hydrodynamic Navier-Stokes (N-S) equations in the following Lagrangian form as:

$$\frac{D\rho}{Dt} + \rho\nabla\cdot\mathbf{v} = 0 \tag{1}$$

$$\frac{D\mathbf{v}}{Dt} = -\frac{1}{\rho}\nabla P + \nu\nabla^2\mathbf{v} + \mathbf{g} \tag{2}$$

where t is the time, ρ is the density, $\mathbf{v}$ is the flow velocity vector, P is the pressure, v is the viscosity coefficient, and $\mathbf{g}$ is the gravitational acceleration.

As reviewed by Monaghan (1994), the SPH formulations are based on the concept of integral interpolations. By using a kernel function to relate the interactions of the fluid particles, differential operators in the Eqs. (1) and (2) are approximated by the summations over the discrete particles. Each individual particle carries the information such as the velocity, density, mass, pressure and other flow variables over the time. Both WCSPH and ISPH numerical schemes solve Eqs. (1) and (2) and the main difference between the two is the solution of fluid pressure. The former uses an explicit equation of state, while the latter uses a semi-implicit pressure Poisson equation. An overview of the fundamental algorithms of the two different SPH methods can be easily found in numerous literatures, e.g. Monaghan (1994) and Cummins and Rudman (1999), so they are not repeated here. One distinctive advantage of the SPH modelling approach is that the extension of the computational program from 2D to 3D is straightforward, although some special considerations are needed to treat the solid boundary conditions. For the ISPH method, we will discuss two different versions, i.e. the density-invariant ISPH (ISPH_DI) and the velocity divergence-free ISPH (ISPH_DF). In ISPH_DI approach, the source term of the pressure equation is the variation of particle densities, while the divergence of intermediate particle velocity fields is used in the ISPH_DF approach (Asai *et al.*, 2012). We will also introduce a modified SPH formulation of the PPE Laplacian operator aiming to improve the ISPH model accuracy and stability.

Our computational experiences found that the ISPH models using the first-order approximation of the Laplacian operator (Shao and Lo, 2003) could converge and produce accurate results in most 2D flow applications with relatively simple geometry, but the stability and accuracy might degrade in 3D simulations, especially near the free surfaces and solid boundaries. Recently, Khayyer and Gotoh (2010; 2012) proposed various higher-order approximations of the Laplacian operator in their MPS methods to improve the pressure predictions, which are quite useful for the development of more accurate ISPH equations. On the other hand, Schwaiger (2008) proposed another discretised form of the Laplacian based on the gradient approximation commonly used in the thermal problems, which retains the higher-order terms in the Taylor series expansion. We would incorporate this in our 3D ISPH model, as this formulation provides a modest improvement to the Laplacian approximation, while remains relatively simple and efficient in the numerical implementations. The final corrected Laplacian approximation for the left-hand side of the PPE is:

$$\nabla\cdot\left(\frac{1}{\rho}\nabla P\right)_i \approx \sum_j \frac{m_j}{\rho_j}\left(\frac{1}{\rho_i}+\frac{1}{\rho_j}\right)(P_i - P_j)\frac{\mathbf{r}_{ij}\cdot\nabla_i W_{ij}}{\mathbf{r}_{ij}^2} - \frac{2}{\rho_i}\nabla(P_i)\cdot\left[\sum_j \frac{m_j}{\rho_j}\cdot\nabla_i W_{ij}\right] \tag{3}$$

The second term on the right-hand side of above equation was derived by following the so-called SPH2 principle in Schwaiger (2008). By reproducing a patch test in Schwaiger (2008), we found that the corrected formulation of Eq. 3 is able to improve the Laplacian estimation on the solid boundaries by 50% as compared with the original formulation in Shao and Lo (2003) for the different test functions. Computationally, it has also been found that by using the new formulation the CPU time can be reduced by 10% in a dam-break flow running against vertical wall (Jian, 2013). This is due to that the improved formulation could reduce the convergence time of the pressure solver, since non-uniformity of the particles was reduced leading to a more stable linear equation system.

BOUNDARY CONDITIONS

For the solid boundary, the dummy particle method proposed by Koshizuka *et al*. (1998) and Gotoh and Sakai (1999), is widely used in the SPH simulations due to its ease of implementation and sufficient accuracy. We also adopt this in the present 3D ISPH computations. For the WCSPH computations in this paper, the standard repulsive boundary proposed by Monaghan (1994) is used. One major difference between the ISPH and WCSPH numerical schemes is that the surface particles need to be identified for solving the PPE in the former. Then the pressure of the surface particles is set to zero as the known boundary condition. In the ISPH_DF method, the surface particles are usually identified by the divergence of particle positions after the prediction step. As for the ISPH_DI method, a particle can be easily regarded to be at the free surface if its density becomes less than 10% of the reference value (Shao and Lo, 2003).

COMPARISONS OF WCSPH AND ISPH SIMULATIONS FOR AN IDEALIZED 2D DAM-BREAK FLOW

In this section, an idealized two-dimensional dam-break flow over a dry bed is investigated using the WCSPH and ISPH models. The water column is initially 0.2 m wide and 0.4 m high, which is released instantaneously into a water tank of 0.8 m long and 0.8 m high at time t = 0.0 s. A total simulation time of 4.0 s is used to study the evolution of the free surface and pressure field over the time. Both SPH models use a particle spacing Δr = 0.005 m. The computational time step Δt is 5.0×10^{-5} s in WCSPH and 5.0×10^{-4} s in ISPH. The former uses the repulsive particles and the latter uses three layers of the dummy particles for the solid wall boundary.

The time histories of the particle snapshots with pressure contours computed by the WCSPH, ISPH_DI and ISPH_DF models are shown in Fig. 1(a) ~ (b), respectively, at different time instants. It is shown that all the three models produce very similar surface and pressure patterns before the water front impacts on the right solid boundary. The propagation speed of the collapsed water column is very similar for the three numerical predictions. The abnormal "sticky particle" phenomenon appears in the WCSPH surface profiles at time t = 0.2 s and 0.4 s in Fig. 1(a), indicated by the fact that some water particles near the left wall boundary fall at a much slower speed than the adjacent water particles. In contrast, both ISPH models are free of this error. The computations show that the water front reaches the right wall boundary at t = 0.32 s. The subsequent upward movement and breaking process affect the stability of the SPH predictions. All three models exhibit some levels of instability in the free surface profiles as the particle configurations have become highly distorted. The surface profiles in Fig. 1(b) display obvious numerical noises as the overturning water front breaks onto the water layer underneath. In particular, the computations of ISPH_DI model show a large number of water particles scattering in the air. On the other hand, the WCSPH profiles suggest a high level of artificial viscosity effect in the modelling, since the scattered particles tend to stick together.

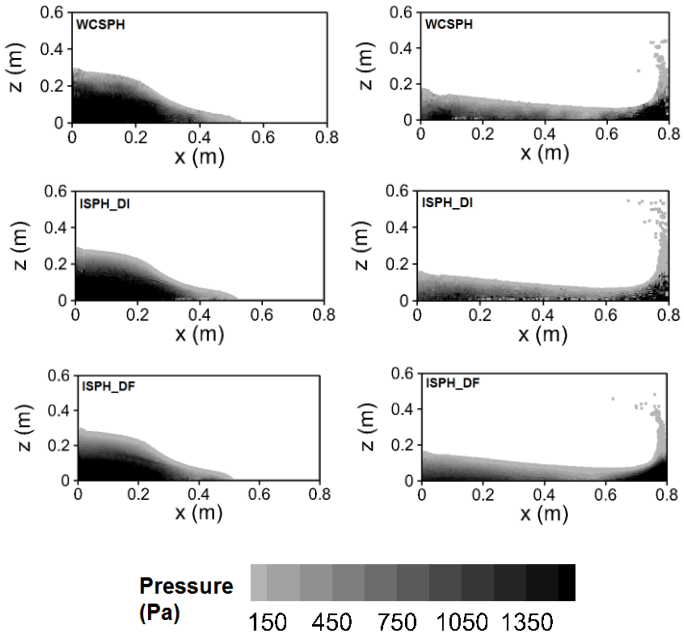

Fig. 1(a) Surface profiles with pressure contours simulated by WCSPH (top), ISPH_DI (middle) and ISPH_DF (bottom) models at t = 0.2 s (left) and 0.4 s (right).

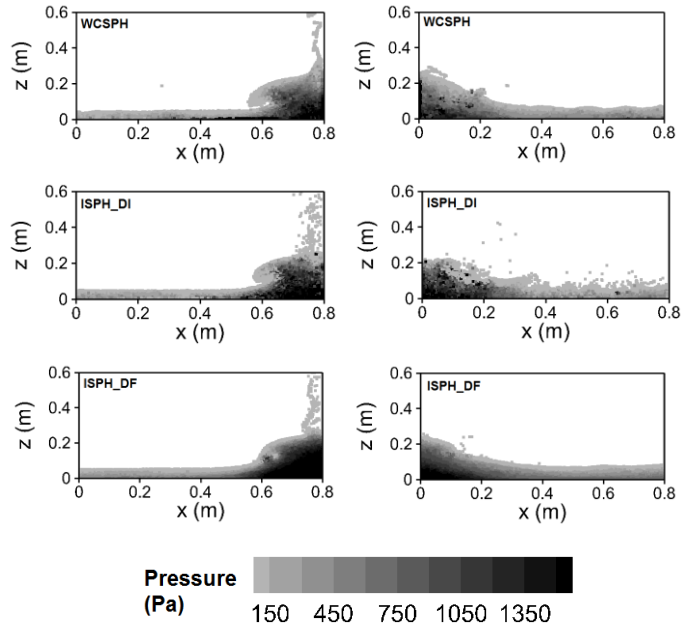

Fig. 1(b) Surface profiles with pressure contours simulated by WCSPH (top), ISPH_DI (middle) and ISPH_DF (bottom) models at t = 0.85 s (left) and 1.55 s (right).

The pressure fields are significantly affected by the breaking in the flow domain. The WCSPH results contain a number of pressure fluctuations in the breaking region, especially close to the solid boundaries. Fig. 1(a) and (b) suggest that there also exist some random fluid particles inside the water that carry larger pressure values than the neighbors. The ISPH_DI results again exhibit strong instability when the wave front strikes at the solid boundary. The pressure field, although still maintains a reasonable distribution over the depth, becomes significantly noisy because of the chaotic surface profile. This is fully demonstrated at t = 0.85 s and 1.55 s in Fig. 1(b). Among the three models, the ISPH_DF model is able to reproduce a relatively smooth and stable pressure field even under the severe breaking. The pressure contours contain very little localized maxima inside the flow domain. Khayyer and Gotoh (2010) also experienced the instability issue of the ISPH_DI in the dam break flow over a wet bed. Later they found that the performance of ISPH_DI could be significantly improved by using a higher-order Laplacian formulation and dynamic error-compensating source term (Khayyer and Gotoh, 2011).

The CPU times required to simulate 4.0 s of flows are 15.75 min, 38.79 min and 37.34 min for the WCSPH, ISPH_DI and ISPH_DF approaches, respectively. It suggests that the WCSPH model is computationally more efficient. The ISPH_DI model requires a slightly higher CPU time than the ISPH_DF model due to the particle disorders which cause larger density errors. If overall computational time and numerical accuracy are taken into account, the ISPH_DF model outperforms the ISPH_DI model, thus only it will be used in the following 3D flow studies as the representative ISPH model.

The dam-break flow has become a widely-used benchmark test for shock-capturing and interfacial flow models. Due to its Lagrangian description, the SPH method has inherent advantages in modelling these flows. However, the SPH application to 3D dam-break flow interactions with a structure has been limited. In contrast, extensive MPS simulations have been carried out by Khayyer and Gotoh (2012). In the following two sections, the WCSPH and ISPH models as discussed in the preceding sections are applied to the three-dimensional dam-break problems. Firstly, a dam-break flow over the fixed object is simulated to validate the models against some reference data. Then, this is followed by an application example considering a movable structure that is subjected to the water impact force and bed frictional force. The capabilities of the two SPH models are investigated through their predictions of the surface evolution, pressure field and hydrodynamic loading on a small object located in the dam-break flow path.

MODEL APPLICATION I - THREE-DIMENSIONAL DAM-BREAK FLOW WITH A FIXED STRUCTURE

Computational domain and model parameters

A 3D dam-break flow with a small fixed obstacle inside the computational domain is used to validate the 3D WCSPH and ISPH models. The corresponding physical experiment was conducted by Kleefsman *et al*. (2005). Fig. 2 shows the experimental setup and the monitoring locations for the water height and fluid pressure, indicated by H_1 - H_4 and P_1 - P_8, respectively. The water tank has a dimension of 3.22 m × 1.00 m × 1.00 m. The initial water column in the reservoir has a dimension of 1.22 m × 1.00 m × 0.55 m. The gate is assumed to open instantaneously. Inside the water tank, a box of size 0.40 m × 0.16 m × 0.16 m is placed at 1.248 m downstream of the gate. Four water depth probes are installed in the flow domain to monitor the water level variations and the box is fitted with eight pressure sensors with four on the front and another four on the top. A total simulation time of 5.0 s is carried out using both the 3D WCSPH and ISPH models. The number of fluid particles used in the simulation is approximately in the order of 100,000 with a particle spacing of Δr = 0.0183 m. A computational time step of $\Delta t = 1.0 \times 10^{-4}$ s and 1.0×10^{-3} s is used for the WCSPH and ISPH models, respectively. Four layers of the dummy particle are used to treat the solid boundaries in the 3D ISPH model, as compared with the three layers used in 2D, following the stability study by Gotoh *et al*. (2005) in their 3D MPS analysis.

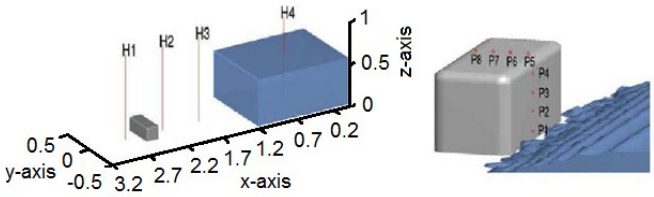

Fig. 2 Schematic setup of experiment and monitoring locations, redrawn from Kleefsman *et al*. (2005).

Result discussions

The 3D WCSPH/ISPH simulated snapshots of the water body deformation are compared with the VOF results of Kleefsman *et al*. (2005) in Fig. 3, at time t = 0.40 s and 0.56 s, respectively. The pressure contours are also included in the SPH particle distributions. The general agreement between the two SPH predictions and the results from Kleefsman *et al*. (2005) is quite satisfactory at both time instants. The SPH computations show slightly slower flow propagation along the tank bottom than the VOF results. The height of splashed water in front of the box varies slightly between the results of the SPH and VOF models. Also the ISPH model tends to predict a larger splash than the WCSPH model but with more stable water front. Consistent with the previous 2D studies, the pressure contours computed by the ISPH model display much less pressure fluctuations than those in the WCSPH results.

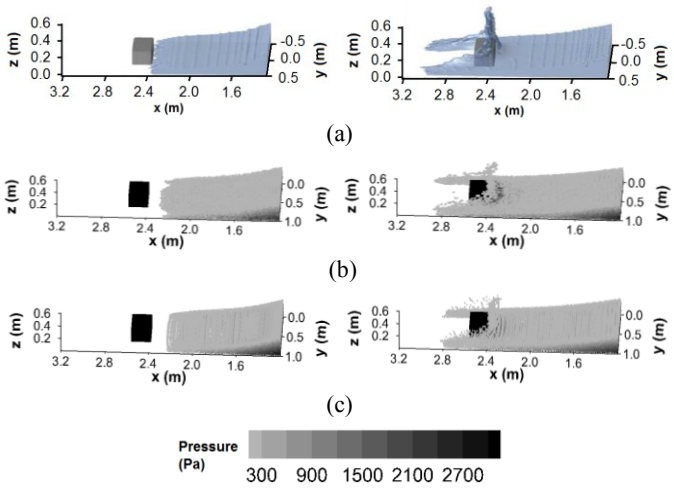

Fig. 3 Snapshot profiles of dam break flow at t = 0.40 s (left) and 0.56 s (right), with (a) VOF results redrawn from Kleefsman *et al*. (2005), (b) 3D WCSPH and (c) 3D ISPH.

Fig. 4 shows the time evolutions of the water height at two measuring points H_2 and H_4. The water heights have been calculated according to the locations of the highest surface particles but excluding the splashed and dispersed ones. The key features in the experimental results have been captured by both SPH models. A slightly delayed arrival of the wave front is noticed in both locations, which is consistent with the slower propagation speed of the water observed in Fig. 3. For the water level variations in front of the small box (H_2), the discrepancy between the experimental and numerical results mainly lies during t = 1.5 s ~ 2.5 s. This corresponds to the arrival of the reflected wave from the left solid boundary at the obstacle. The ISPH results show a milder reduction in the water height after t = 2.5 s. At the reservoir area H_4, the water height profiles demonstrate a satisfactory agreement between the experimental and numerical results until t = 2.6 s. The gradual decrease of the water height during this period as well as the later two maxima caused by the reflected waves are well captured by both SPH models. However, the second local maxima around t = 4.0 s is underestimated by the numerical models. In spite of the over-prediction of the first maxima and the under-prediction of the second maxima, the predicted water heights by the ISPH model are generally comparable to those by the WCSPH model. As will be seen later, however, the ISPH predictions demonstrate much better accuracy in terms of the pressure distribution.

.

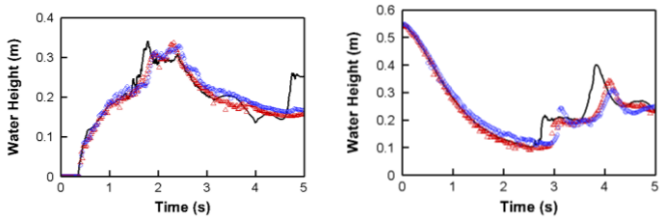

Fig. 4 Time evolutions of water height at H_2 (left) and H_4 (right), computed by 3D WCSPH (triangle) and ISPH (circle) models with experimental data (solid line) of Kleefsman *et al.* (2005).

The computed pressure records at P_2 and P_4, both on the front surface of the box, and P_5 and P_7, both on the top surface of the box, are shown in Fig. 5(a) ~ (d), respectively. The comparisons are made between the WCSPH/ISPH results and the experimental data of Kleefsman *et al*. (2005). It is shown that the WCSPH results contain severe fluctuations in the pressure predictions when the large hydrodynamic impacts occur, while the ISPH results are much more reasonable due to its true hydrodynamic formulation to solve the fluid pressures. From Fig. 5(a) ~ (b), it is seen that the agreement between the SPHs and experimental results is quite good at the two measuring points on the front face of the box. At this location, the pressure fields are not much influenced by the splashed particles, so the pressure variations are expected to be smooth. The ISPH model only slightly under-estimates the pressures between t = 0.5 s and 2.3 s. However, the second increase in the experimental pressure is not well reproduced by the numerical models during t = 4.6 s ~ 5.0 s, which is thought to be caused by the delay in the wave front arrival. On the other hand, the pressure comparison on the top surface of the box in Fig. 5(c) ~ (d) shows relatively larger disagreements between the numerical and experimental data. One reason could be due to that the turbulence effect is not considered by the present model, as the water splash is more predominant in this region. Another reason could be the entrainment of the air, which has not been adequately accounted for by the present single-phase algorithms. As for the falling of the water droplets onto the top surface of the box, the pressure is expected to experience certain degrees of the fluctuation. These fluctuations are drastically overestimated by the WCSPH model. Overall the ISPH computations perform much better in producing a realistic pressure variation pattern. In consistency with the under-prediction of the water heights around t = 5 s as shown in the left graph of Fig. 4, Fig. 5 shows that both SPH models underestimate the pressure around the object at this instant.

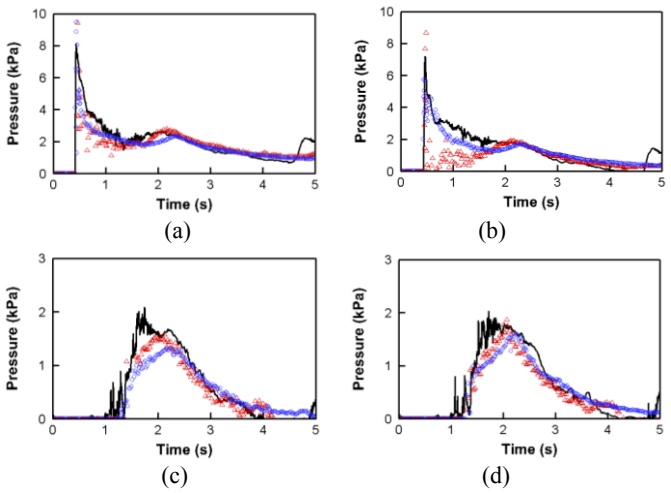

Fig. 5 Time evolutions of pressure at (a) P_2, (b)P_4, (c) P_5 and (d) P_7, computed by 3D WCSPH (triangle) and ISPH (circle) models with experimental data (solid line) from Kleefsman *et al.* (2005).

MODEL APPLICATION II - THREE-DIMENSIONAL DAM-BREAK FLOW WITH A MOVABLE STRUCTURE

Although several SPH applications are found in the literatures to investigate the dam-break flow interactions with fixed structures, very little work has been reported concerning the movable ones, in spite of the fact that large amount of debris can be generated by severe flooding which move with varying degree of freedom. It is promising to note that good progress has been made in recently years to understand the fundamentals of this phenomenon, as reported in Liang *et al.* (2010), Chen *et al*. (2013) and Liu *et al*. (2014). More practical scenarios have been considered by Wu *et al*. (2013), using a GPU-based WCSPH model to simulate dam-break flooding in urban areas.

Model setup and computational parameters

Here the small structure box placed downstream of the dam as shown in Fig. 2 is considered to be movable. Once the horizontal component of the impact forces exceeds the frictional force between the obstacle and the floor, the box will slide. In order to reduce the complexity involved in the study, the frictional coefficient is set to be constant under both the static and dynamic conditions. Apart from the frictional coefficient, the other free parameters in the simulation include the mass of the box. In our numerical experiment, different values of the mass are assigned, ranging from 100 kg ~ 700 kg. In the computations, the solid wall located at the downstream end of the tank (x = 3.22 m) is removed to ensure no wave reflections. A total physical time of 2.0 s is simulated in all the cases, which is long enough to capture the maximum hydrodynamic loading on the front surface of the box and disclose main characteristics of the box motion.

Movable structure model

When being subject to the hydrodynamic loading, the movable box experiences two opposing forces, i.e. the hydrodynamic force caused by the fluid pressure differences between the upstream and downstream faces and the frictional force arising from the channel bed. The shear force on the other faces of the box is assumed to be negligible compared with the pressure force. Considering the symmetrical configuration of the problem in the y direction, the box is allowed to move only in the longitudinal x direction with one degree of freedom. The frictional force exerted on the movable box is simply calculated as follows:

$$f_{friction} = \alpha m_{box} \tag{4}$$

where α is the frictional coefficient, which is fixed as 0.3 in the present study; and m_{box} is the mass of the box. The acceleration of the box is thus calculated by

$$\begin{cases} a_{box,horizontal} = \dfrac{F_{surf} - f_{friction}}{m_{box}}, \text{ if } F_{surf} > f_{friction} \\ a_{box,horizontal} = \dfrac{F_{surf} - f_{friction}}{m_{box}}, \text{ if } F_{surf} < f_{friction} \text{ and } u_{box,horizontal} > 0 \\ a_{box,horizontal} = 0.0, \text{ if } F_{surf} < f_{friction} \text{ and } u_{box,horizontal} = 0 \end{cases} \tag{5}$$

where F_{surf} is the fluid impact force acting on the structure surface, and $a_{box,horizontal}$ and $u_{box,horizontal}$ are the acceleration and velocity of the movable box in stream-wise direction, respectively.

Here we should note that due to the negligence of buoyancy and uplift force in the numerical model, the simulations could underestimate the velocity and displacement of the movable structure. However, this underestimation only occurs when there exists a gap between the bottom of the structure and the bed.

Result and discussions

To make a reference comparison, we first assume the structure to be stationary and compute the x-component of the hydrodynamic forces by the WCSPH and ISPH models as shown in Fig. 6. The force is an integration of the pressure over the surface areas, so it varies much more smoothly than the pressure profile. The figure shows that a reasonably good agreement is observed between the two SPH modeling results. Both force curves show a pattern consisting of a sharp rise at t = 0.4 s when the dam-break flow hits on the front surface of the box, followed by a gradual decrease after t = 0.55 s. The maximum impact force experienced by the box is predicted to be slightly higher in the ISPH computations. While both models display some levels of fluctuation in their predictions, the force curve produced by the ISPH model is much less noisy. The WCSPH force curve undergoes relatively large rises and drops after t = 0.55 s, then producing a steeper decrease of the force pattern than the ISPH result.

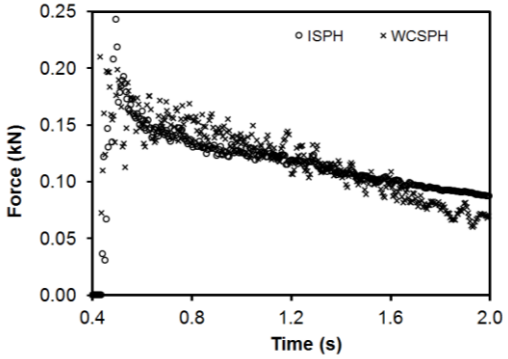

Fig. 6 Hydrodynamic forces on fixed box computed by two SPH models.

After the static box test, the structure is treated as movable and the hydrodynamic forces and horizontal velocity variations simulated by the SPH models are summarised in Figs. 7 and 8, respectively, with the different box mass settings. The force curves in Fig. 7 suggest that the reduction in the impact forces is noticeable when the box mass is reduced to a very low level, i.e. m_{box} = 100 kg. The force curves for other masses remain largely unchanged from the fixed-box case, indicating that the moving velocity of the box of the larger mass is too small to effectively offset the impact load, given that the dimensions of the box are kept the same. The effect of the box movement becomes evident only when the box moves with a sufficiently high speed. Since the structure movement helps to reduce the water run-up height in the front, the box that moves faster is expected to incur smaller pressure forces on its front surface. Since all the boxes are initially kept stationary and those with bigger masses come to a stop very quickly, the forces in these situations are not very different from the fixed-box case. In the gradual force reduction phase, boxes with smaller mass settings tend to have a steeper slope in their impact force curves. In this study, the mass of the box is reduced from 700 kg to 100 kg with a constant interval. It can be seen that the differences in the impact force curves increase with the decreasing mass values. Besides, it clearly demonstrates that even under the movable structure condition, the ISPH model still predicts a much more stable force history than the WCSPH model. The results with 100 kg and 200 kg mass computed by ISPH show some degrees of sudden change around t = 1.2 s, because this is the moment when the reflected wave suddenly plunges onto the top of the structure. The WCSPH simulations do not demonstrate such a sudden change, because its predicted force contains excess fluctuations that somewhat submerge the physical change of the impact force, given that this sudden change is not significant.

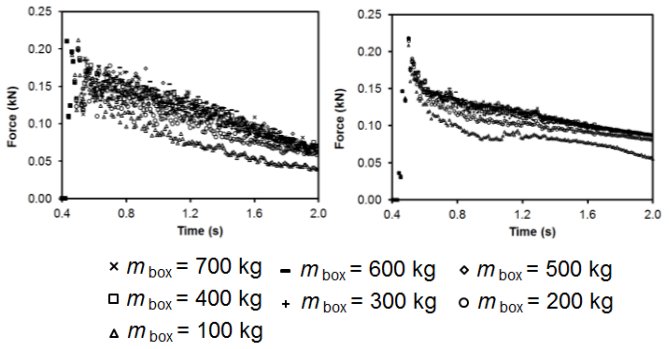

Fig. 7 Hydrodynamic forces on movable structure computed by WCSPH (left) and ISPH (right) models.

In terms of the horizontal velocity variations, Fig. 8 shows that the boxes heavier than 500 kg behave almost like a fixed structure with little movement under the fluid impact (the curves of m_{box} = 600 kg and 700 kg are not shown in the figure, as no tangible motion is found). The boxes with m_{box} < 500 kg are all moved upon the strike of the dam-break flood, and then decelerate before eventually coming to a stop. The flood wave arrives at the front face of the box at around t = 0.4 s, when the motion of the box is initiated. The smaller the mass is, the bigger acceleration it obtains. The fluid forces should gradually decrease with the emptying of the reservoir, while the frictional force remains constant as long as the velocity of the box is not zero. When the hydrodynamic force is just balanced by the bed friction, the box velocity reaches the peak value. Then the box starts to decelerate and finally stop. The box velocity returns to zero by about t = 1.23 s and 1.83 s for m_{box} = 500 kg and 400 kg, respectively, in the WCSPH computations. In comparison, these timelines are 1.10 s and 1.57s respectively, in the ISPH results. Because of the limited computational domain and simulation time, the boxes with smaller mass have not stopped at the end of the current simulations. As the mass of the boxes reduces, the adjacent curves become increasingly separated, signifying that the movement of the box is very sensitive to the box mass for the lighter ones. If superposing the WCSPH and ISPH results together and examining their hydrodynamic forces and velocity differences, we could easily note that the WCSPH model generally predicts a higher hydrodynamic load than the ISPH model, thus leading to a faster structure movement.

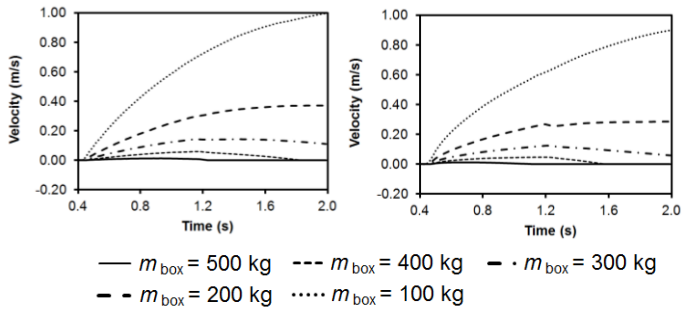

Fig. 8 Horizontal velocities of movable structure computed by WCSPH (left) and ISPH (right) models.

CONCLUSIONS

The paper presents 3D WCSPH & ISPH studies on the dam-break flow interactions with fixed and movable structures, and aims to make a comparison between the two modelling techniques. Both WCSPH and ISPH computations of the fixed structure case provide reasonable agreements with the experimental observations, but the ISPH simulations demonstrate an improved prediction of the water splash and pressure field. Numerical experiments were then designed to study the response of a movable structure subject to the same dam-break flow. Again, the ISPH model demonstrated better performance in predicting the hydrodynamic loads. It has been found that the mass of the movable obstacle plays an important role in its response to the flow impact. With a larger mass, the obstacle does not become mobilized easily and the phenomenon returns to the fixed-obstacle case, while with a smaller mass the movement of the obstacle is highly sensitive to the mass. Regarding the CPU cost, 2D/3D WCSPH and ISPH models are comparable in most cases considered in this paper. Hence, we conclude that the 3D ISPH model could possess the same computational feasibility as the WCSPH counterpart, at least for the low-medium particle resolutions as investigated in present study.

However, we would like to point out that the scaling of CPU time with the increased particle resolution may be different between these two SPH models. In case of very large particle systems, the WCSPH model could become more efficient due to that the CPU load for solving the PPE in the ISPH model overwhelmingly overweighs the computational expenses in the WCSPH model. The search for neighboring particles and the predictor-corrector algorithms of the two methods have nearly the same CPU expenses. The ISPH can use a time step at least five times larger (Violeau and Leroy, 2015), but this is not enough to offset the cost for solving the pressure Poisson equation. The availability of more efficient linear solver and advanced computing environment may make ISPH promising even under very high particle resolutions as well. On the other hand, further

enhancement of the WCSPH numerical scheme by using the concepts of error compensation pressure or kernel correction of viscosity [e.g. Khayyer and Gotoh (2010a; 2010b)] could make this model equally attractive.

ACKNOWLEDGEMENTS

The first author acknowledges the Jafar Studentship for her PhD study at University of Cambridge. We thank the Open Research Fund of the State Key Laboratory of Hydraulics and Mountain River Engineering, Sichuan University (SKHL1404; SKHL1409).

REFERENCES

Amicarelli, A, Albano, R, Mirauda, D, Agate, G, Sole, A and Guandalini, R (2015). "A Smoothed Particle Hydrodynamics Model for 3D Solid Body Transport in Free Surface Flows," *Comp & Fluids*, 116, 205–228.

Asai, M, Aly, AM, Sonoda, Y and Sakai, Y (2012). "A Stabilized Incompressible SPH Method by Relaxing the Density Invariance Condition," *J Appl Math.*, Article ID 139583.

Bouscasse, B, Colagrossi, A, Marrone, S and Antuono, M (2013). "Nonlinear Water Wave Interaction with Floating Bodies in SPH," *J Fluids & Struc*, 42, 112-129.

Canelas, RB, Domínguez, JM, Crespo, AJ, Gómez-Gesteira, M and Ferreira, RM (2015). "A Smooth Particle Hydrodynamics Discretization for the Modelling of Free Surface Flows and Rigid Body Dynamics," *Int. J. Numer. Meth. Fluids*, 78(9), 581–593.

Chen, Z, Zong, Z, Liu, MB and Li, HT (2013). "A Comparative Study of Truly Incompressible and Weakly Compressible SPH Methods for Free Surface Incompressible Flows," *Int J Numer Meth Fluids*, 73(9), 813-829.

Cummins, SJ, and Rudman, M (1999). "An SPH Projection Method," *J Comput Phys*, 152, 584-607.

Ferrari, A, Dumbser, M, Toro, EF and Armanini, A (2009). "A New 3D Parallel SPH Scheme for Free Surface Flows," *Comput Fluids*, 38(6), 1203-1217.

Gómez-Gesteira, M and Dalrymple, RA (2004). "Using a 3D SPH Method for Wave Impact on a Tall Structure," *J Waterw Port Coast Ocean Eng*, 130(2), 63-69.

Gotoh, H, Ikari, H and Sakai, T (2005). "Development of Numerical Wave Flume by 3D MPS Method," *Proc 5th Int Symp Waves 2005, Ocean Waves Measurement and Analysis*, Madrid, Spain, paper number 196.

Gotoh, H and Sakai, T (1999). "Lagrangian Simulation of Breaking Waves using Particle Method," *Coast Eng J*, 41, 303-326.

Hu, XY and Adams, NA (2009). "A Constant-density Approach for Incompressible Multi-phase SPH," *J Comput Phys*, 228, 2082-2091.

Jian, W (2013). *Smoothed Particle Hydrodynamics Modelling of Dam-break Flows and Wave-structure Interactions*, Ph.D. Thesis, University of Cambridge.

Khayyer, A and Gotoh, H (2010a). "A Higher Order Laplacian Model for Enhancement and Stabilization of Pressure Calculation by the MPS Method," *Appl Ocean Res*, 32(1), 124-131.

Khayyer, A and Gotoh, H (2010b). "On Particle-based Simulation of a Dam Break over a Wet Bed," *J Hydraul Res*, 48(2), 238-249.

Khayyer, A and Gotoh, H (2011). "Enhancement of Stability and Accuracy of the Moving Particle Semi-implicit Method," *J Comput Phys*, 230 (8), 3093-3118.

Khayyer, A and Gotoh, H (2012). "A 3D Higher Order Laplacian Model for Enhancement and Stabilization of Pressure Calculation in 3D MPS-based Simulations," *Appl Ocean Res*, 37, 120-126.

Kleefsman, KMT, Fekken, G, Veldman, AEP, Iwanowski, B and Buchner, BA (2005). "Volume-of-fluid Based Simulation Method for Wave Impact Problems," *J Comput Phys*, 206, 363-393.

Koshizuka, S, Nobe, A and Oka, Y (1998). "Numerical Analysis of Breaking Waves using the Moving Particle Semi-implicit method," *Int J Numer Meth Fluids*, 26, 751-769.

Liang, D, Thusyanthan, I, Madabhushi, SPG and Tang, H (2010). "Modelling Solitary Waves and Its Impact on Coastal Houses with SPH Method," *China Ocean Eng*, 24(2), 353-368.

Liu, MB, Shao, JR and Li, HQ (2014). "An SPH Model for Free Surface Flows with Moving Rigid Objects," *Int J Numer Meth Fluids*, 74, 684-697.

Monaghan, JJ (1994). "Simulating Free Surface Flows with SPH," *J Comput Phys*, 110, 399-406.

Ren, B, He, M, Dong, P and Wen, H (2015). "Nonlinear Simulations of Wave-induced Motions of a Freely Floating Body Using WCSPH Method," *Appl Ocean Res*, 50, 1-12.

Schwaiger, HF (2008). "An Implicit Corrected SPH Formulation for Thermal Diffusion with Linear Free Surface Boundary Conditions," *Int J Numer Meth Eng*, 75, 647-671.

Shao, SD and Lo, EYM (2003). "Incompressible SPH Method for Simulating Newtonian and Non-Newtonian Flows with a Free Surface," *Adv Water Resour*, 26, 787-800.

Violeau, D and Leroy, A (2015). "Optimal time step for incompressible SPH," *J Comput Phys*, 288, 119-130.

Wu, JS, Zhang, H and Dalrymple, RA (2013). "Simulating Dam-break Flooding with Floating Objects through Intricate City Layouts Using GPU-based SPH Method," *World Congress on Engineering* 2013, Imperial College of London, July 03-05, 1755-1760.